IEEE Access
Multidisciplinary | Rapid Review | Open Access Journal

Received August 8, 2020, accepted August 13, 2020, date of publication August 18, 2020, date of current version August 28, 2020.

Digital Object Identifier 10.1109/ACCESS.2020.3017460

Finite-Time Disturbance-Observer-Based Integral Terminal Sliding Mode Controller for Three-Phase Synchronous Rectifier

BAHMAN ESKANDARI[1], (Member, IEEE), AMIN YOUSEFPOUR[2], MOOSA AYATI[2], JORMA KYYRA[1], (Member, IEEE), AND EDRIS POURESMAEIL[1], (Senior Member, IEEE)

[1]Department of Electrical Engineering and Automation, Aalto University, 02150 Espoo, Finland
[2]School of Mechanical Engineering, College of Engineering, University of Tehran, Tehran 1417466191, Iran

Corresponding author: Bahman Eskandari (bahman.eskandari@aalto.fi)

ABSTRACT This article is concerned with the design of a finite-time disturbance-observer-based integral terminal sliding mode controller for the effective performance of three-phase synchronous rectifiers. The proposed control technique is developed based on the conventional synchronous reference frame model of the three-phase grid-connected converter, and the system dynamics is described in terms of a time-varying non-linear state equation. The variation of DC-load is considered as a disturbance. Therefore, a combination of a fast disturbance observer and an integral terminal sliding mode controller is utilized to produce the reference value of the direct axis for the current control loop. In this research, by employing Lyapunov stability theorem in the theoretical analysis and by numerical simulations, it is confirmed that the proposed closed-loop system is stable and the states converge to desired values in finite time even in the presence of load disturbance and control input saturation. The integral terminal sliding mode controller is utilized to maintain a robust performance along with a faster response of the converter. In order to demonstrate the performance ability of the proposed control scheme under real condition, an AC power source, impregnated with low order harmonics, is assumed. A real-time laboratory setup of the synchronous rectifier has been developed successfully, and the effective performance of the proposed control technique is fully proven.

INDEX TERMS AC-DC power converters, disturbance observer, integral terminal sliding mode controller.

I. INTRODUCTION

There is a vast area of applications for synchronous three-phase rectifier (SR) in the industrial world such as regenerative motor drives, industrial DC power supplies, common DC bus for multiple drives, and DC traction systems. This type of converter, as a bidirectional power flow controller, is prevalent in the renewable energy market as well. There are three famous reference frames for modeling and control of synchronous converters, natural (abc), rotational ($\alpha\beta$) and stationary (dq). All the advanced control techniques are defined based on one of these frames, which all of them are reviewed in [1]. Each one of three-phase currents is controlled individually in *abc* frame. Generally, direct control of three AC currents can be done in two ways, using a hysteresis modulator (with variable and high switching frequency) or converting sinusoidal current waveforms into voltage type through a proportional resonant controller (PR) for applying to the voltage source converter. However, in [2] the authors have tried to control a four-wire converter in the natural frame to keep the voltage of neutral point stable, due to unbalance and non-linear lodes through the High Order Integral Terminal (HOIT) technique. Using the stationary reference frame ($\alpha\beta$) is the second well-known control technique for SR [3], [4]. In this type of controller, all the AC side's currents are transformed into the stationary reference frame through *abc* to $\alpha\beta$ transform. Because of the sinusoidal nature of currents in the $\alpha\beta$ frame, the conventional Proportional Integral (PI) controller is not capable of compensating the steady-state error. Therefore, employment of a higher-order controller like PR is necessary. In [5], a capacitor optimization along with a ripple compensation technique for DC voltage of SR is proposed based on $\alpha\beta$ theory in unbalanced networks. A direct power control strategy in the $\alpha\beta$ frame for

The associate editor coordinating the review of this manuscript and approving it for publication was Yan-Jun Liu.

three-phase voltage-source rectifiers based on extended-state observation is discussed in [6]. However, the stationary reference frame model is utilized along with the PR controller. The main concern of the PR controller is tracking the fundamental signal in the presence of low order harmonics because of the difficulty of tuning the resonant parameter in polluted AC waveforms.

The third model for SR introduced in the synchronous rotational reference frame (dq), to avoid using PR controller. Because of working with DC values, this is a popular controller for SR [7]–[17], modeling and control of power converters in microgrids have been investigated in [7], and a droop control technique is proposed for active power flow control of converters based on multiple PI controller loops in dq frame. A combination of fuzzy-model-based control and adaptive sliding mode technique has been proposed for the uncertain estimation of a three-phase AC/DC converter in [8]. One of the drawbacks of this method is convergence time. Conventional sliding modes do not assure finite-time convergence. Also, this method does not possess disturbances observer and may not show appropriate performance in uncertain conditions. Controller of parallel three-phase PWM converters under generalized unbalanced operating conditions is developed in dq frame in [9]. The authors found a solution for reducing the amount of zero and negative sequence currents due to the unbalance voltage source. An algorithm for predictive duty cycle control of three-phase active rectifiers has been established in [10]. This technique works by defining an optimization problem. Optimized duty cycles will be obtained by solving the cost function that is defined in the dq frame. The lack of stability analysis is the main challenge of this technique. A sensorless control method is discussed in [11] for a three-phase voltage source rectifier by designing a linear observer for load current along with a feedforward control scheme. For tracking the fast dynamics in the grid-connected converter, utilizing a sliding mode controller is proposed in [12], whereas a parallel integrator is required to eliminate the steady-state error. A current-controlled voltage-mode scheme for distributed energy resource units based on sliding-mode control (SMC) for outer loop and an adaptive terminal sliding mode control in hybrid grid-connected converters involve solar PV and wind systems strategy are proposed in [13] and [14] respectively, with no attention to the stability in the finite time and the presence of saturation. A new approach for control of three-phase SR is proposed in [15], [16], which relies on an extended state observer (ESO)-based second-order sliding mode (SOSM). In this method, two control loops for voltage regulation (outer loop) and instantaneous power tracking (inner loop) are considered. The outer loop is a combination of an H∞ controller and ESO, whereas in the inner loop, SOSM is employed to tune active and reactive power.

There is a wide range of uncertainties in power electronics converters, including the active and passive parameters, inherent delay of measuring and filtering, estimated frequency and phase by PLL, inevitable switching dead time and load disturbances. In order to implement a modern control for a power converter, an effective observer is required to estimate the uncertainty of parameters and disturbances together. Disturbance-observer (DO) mechanism is employed to estimate the total disturbance [17]–[22]. The disturbance observer and terminal sliding mode controller (TSMC) have been developed for tracking control of an uncertain and non-linear system with unknown external disturbance in [23]–[25]. An offset-free model predictive control (MPC) algorithm using a DO to control the power flow of a three-phase SR is developed in [24] in which, a linear observer is designed according to standard Luenberger procedure. The Grid-side converter of a wind generation system is controlled by an evolved form of TSM controller in [25]. In this paper, a conventional PI controller produces the desired active power and corresponding currents (in $\alpha\beta$ frame) for tracking DC voltage, and two loops of Integral Terminal Sliding Mode controllers (ITSMC) are utilized to generate the desired voltage values in $\alpha\beta$ coordinate.

Various types of control methods for SR have been surveyed where the output of the control process in power converter usually is a time-variant rotational vector. This vector is indicated by a modulation index (m) as amplitude, and a power angle (δ), which are limited parameters, and conventional controllers do not have any sense of instability conditions by these limited (saturated) values. This problem can be severe when using consecutive control loops. Among the modern control methods for SR, application of observer-based control techniques along with sliding mode control is known as a robust and more effective solution. From the stability viewpoint, the Lyapunov-based control methods are asymptotically stable, and the steady-state tracking error will be zero in infinite time. The proposed ITSMC method is the main contribution of this paper for the rotating reference frame along with employing disturbance-observer to estimate DC link current. It is mathematically proven that the disturbance approximation error converges to zero in a finite time which is a new concept in error tracking in three-phase bidirectional power converters. The objective of the present study is to improve the proposed method in previous investigations. Advantages of the scheme, proposed in this manuscript, compared to conventional controllers, are listed as:

- The stability of the closed-loop system in the presence of control input saturation. In real-world applications, bounds must be considered for control force. In the proposed controller, using control input saturation, the limitation in the actuators is considered for a three-phase synchronous rectifier. The proposed Lyapunov stability theorem of the disturbance-observer-based TSMC guarantees the stability of the control system.
- Compared to the conventional sliding mode control, the proposed control scheme guarantees the control of the system in the finite time.
- (SMC) generates chattering for uncertain systems due to the presence of sign function in the control input.

Consequently, the chattering causes vibrations in the system because it takes time to converge to the sliding surface. In the present control scheme (ITSMC), however, the disturbance observer will estimate the uncertainties and disturbances. Hence, the chattering in the system will be reduced.

After the introduction, modeling of the SR in both steady-state phasor based and synchronous rotating reference frames along with conventional control loops is explained. In the third part, the theory of ITSMC and DO is developed, and details of controller design are explained. All the simulation and experimental results are compared and presented in the fourth section.

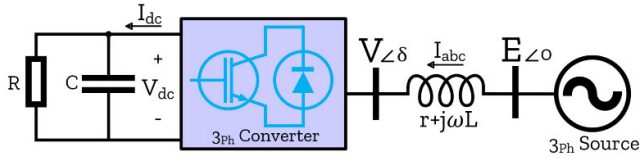

FIGURE 1. Single line diagram of synchronous rectifier.

II. MODELING OF THE SYNCHRONOUS RECTIFIER

A general single line diagram of the synchronous rectifier is shown in Fig. 1. A three-phase voltage source converter is connected to a three-phase source through an interface inductance. The three-phase source could be considered as a THEVENIN equivalent of a network in which series equivalent impedance is merged in interface inductance. DC side consists of a capacitor bank in parallel with a resistive load.

A. COMPLEX POWER FLOW

To have a better understanding of the concept of power flow between converter and network a complex power flow study is required. By assuming an ideal programmable voltage source instead of a real converter in Fig. 1, a single-phase equivalent circuit is drawn in Fig. 2.

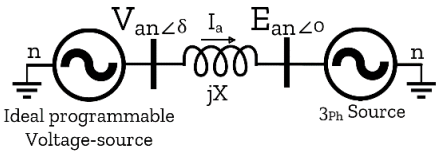

FIGURE 2. Single-phase equivalent circuit of the ideal power converter.

V_{an} and E_{an} are the per phase RMS values of converter and network voltages, respectively, while the resistor of interface inductance is ignored. The three-phase complex power at converter terminal is defined as:

$$S_{3\varphi} = 3V_{an}I_a^* = P + jQ \tag{1}$$

Through a Kirchhoff voltage law, the current equation can be written as:

$$I_a = \frac{|V_{an}|\angle\delta^\circ - |E_{an}|\angle 0^\circ}{|X|\angle 90^\circ} \tag{2}$$

By substituting I_a in (1) and separating real and imaginary parts, active and reactive components of complex power are obtained in:

$$\begin{cases} P = 3\dfrac{|E_{an}|\,|V_{an}|}{|X|}\sin\delta \\ Q = 3\dfrac{|E_{an}|\,|V_{an}|}{|X|}\cos\delta - 3\dfrac{|E_{an}|^2}{|X|} \end{cases} \tag{3}$$

This is a very useful equation for justifying the behaviour of every possible application for a three-phase grid-connected converter with respect to the AC network. In this project, SR application is considered while the ideal value for exchanged reactive power is zero (Q = 0). By considering a fixed value for E_{an} in (3), the trace of V_{an} on E_{an} must be equal to E_{an} to meet the zero reactive power condition, $|V_{an}|\ \cos\ \delta = |E_{an}|$. Subsequently, the vertical trace of V_{an} is assigned to control the amount of active power, $P\ \propto |V_{an}|\sin\delta$. Figure. 3 illustrates the mentioned conditions.

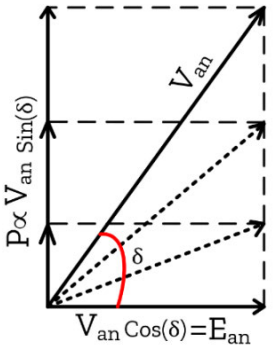

FIGURE 3. Phasor diagram of zero reactive power condition.

In voltage source converters, V_{an} is produced by multiplying the modulation index ($0 < m < 1$) in DC voltage (V_{dc}), $\sqrt{3}V_{an} = mV_{dc}/\sqrt{2}$. It means, by controlling m and power angle (δ) it is possible to keep the reactive power at zero while exchanging active power. However, it should be noted that both δ and m, as control actuators, are limited values with respect to exchanged active power. By considering the maximum value for modulation index ($m = 1$), the minimum allowed value for V_{dc} and maximum permitted value for δ, respect to the amount of active power, are obtained from (4).

$$\begin{cases} 0 = |V_{an}|\cos\delta - |E_{an}| \\ P = 3\dfrac{|E_{an}|\,|V_{an}|}{|X|}\sin\delta \\ \sqrt{3}V_{an} = mV_{dc}/\sqrt{2} \end{cases} \xrightarrow{m=1} \begin{cases} \delta_{max} = \tan^{-1}\left(\dfrac{PX}{3E_{an}^2}\right) \\ V_{dcmin} = \sqrt{\dfrac{2P^2X^2}{3E_{an}^2} + 6E_{an}^2} \end{cases} \tag{4}$$

This is an important equation, which indicates the criteria of stable and feasible operation of the converter. As an example, for $X = 0.5\Omega$ and $E_{an} = 23\text{V}$ the profile of V_{dc-min}

and δ_{max} respect to exchanged active power ($\pm 5kW$) are illustrated in Fig. 4.

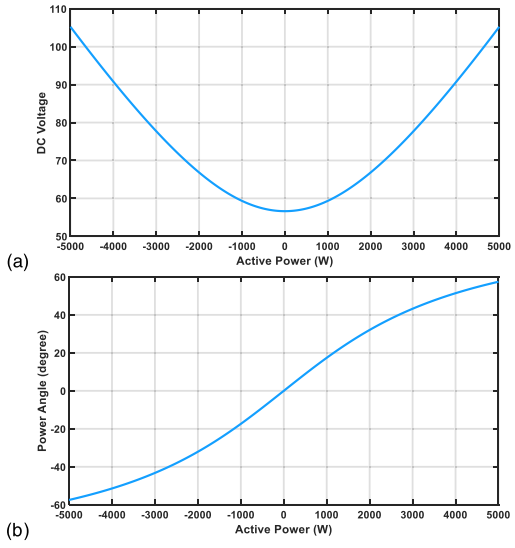

FIGURE 4. Profile of V_{dc-min} (a) and δ_{max} (b) respect to exchanged active power.

B. DYNAMIC MODEL AND CONTROL OF SR

By considering all the AC side parameters of SR in Fig. 1, a set of per-phase differential equations can be written as (5) in *abc* frame, which they have sinusoidal time-variation.

$$L\frac{di_{abc}}{dt} + ri_{abc} = E_{abc} - V_{abc} \tag{5}$$

By applying *abc/dq* transform (6) and changing the rotational reference frame in (5), two stationary and orthogonal equations with dc components are appeared in (7).

$$\begin{bmatrix} x_d \\ x_q \end{bmatrix} = \begin{bmatrix} \cos\omega t & \sin\omega t \\ -\sin\omega t & \cos\omega t \end{bmatrix} \begin{bmatrix} \frac{2}{3} & \frac{-1}{3} & \frac{-1}{3} \\ 0 & \frac{1}{\sqrt{3}} & \frac{-1}{\sqrt{3}} \end{bmatrix} \times \begin{bmatrix} x_a \\ x_b \\ x_c \end{bmatrix} \tag{6}$$

$$\begin{cases} E_d = V_d + ri_d + L\dfrac{di_d}{dt} - L\omega i_q \\ E_q = V_q + ri_q + L\dfrac{di_q}{dt} + L\omega i_d \end{cases} \tag{7}$$

where, ω is the frequency of the AC power network, which is extracted from the Phase Locked Loop (PLL). The abc/dq transform is here to emphasize the important role of the PLL to extracting the instantaneous phase angle. In almost all articles, it is assumed that the phase value is ideally available without any uncertainty. Indeed, ωt must be considered as an impregnated signal with unknown disturbance. The definition of active power in the *dq* frame is changed to (8). By ignoring converter losses, the AC side active power is equal to the DC side:

$$P = \frac{3}{2}\left(V_d i_d + V_q i_q\right) = V_{dc} I_{dc} \tag{8}$$

The differential equation of the DC side (9) is obtained through a simple current law at DC point.

$$I_{dc} = C\frac{dV_{dc}}{dt} + \frac{V_{dc}}{R} \tag{9}$$

Assuming a balanced three-phase source as reference leads to having only the direct axis component of E_d while the other component is zero ($E_q = 0$). After substituting (9) in (8), the non-linear state-space equation (10), which describes the dynamic behaviour of SR, can be derived from (7-9).

$$\frac{d}{dt}\begin{bmatrix} i_d \\ i_q \\ V_{dc} \end{bmatrix} = \begin{bmatrix} \frac{-r}{L} & \omega & \frac{-V_d}{L} \\ -\omega & \frac{-r}{L} & \frac{-V_q}{L} \\ \frac{3V_d}{2CV_{dc}} & \frac{3V_q}{2CV_{dc}} & \frac{-1}{RC} \end{bmatrix} \times \begin{bmatrix} i_d \\ i_q \\ V_{dc} \end{bmatrix} + \begin{bmatrix} \frac{1}{L} \\ 0 \\ 0 \end{bmatrix} E_d \tag{10}$$

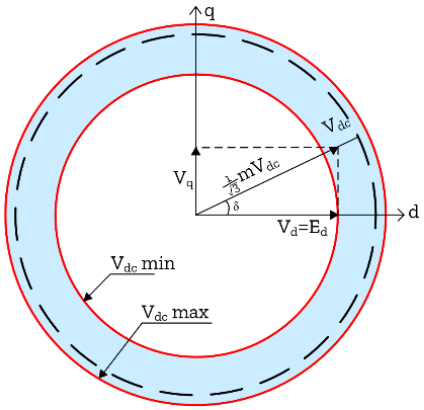

FIGURE 5. Vector diagram between the terminal voltage of converter and power network in *dq* frame.

During the transformation from *abc* to *dq* the power angle δ remains intact and is transferred without changing. This concept is illustrated in Fig. 5, while the range of V_{dc} is indicated by solid lines and dashed line, is the desired DC voltage. In other words, the voltage decomposition in the converter terminal (V_d and V_q) is written as:

$$\begin{cases} V_d = \dfrac{mV_{dc}}{\sqrt{3}}\cos\delta \\ V_q = \dfrac{mV_{dc}}{\sqrt{3}}\sin\delta \end{cases} \tag{11}$$

By replacing (11) in (10), a new state-space equation is appeared (12). Both m and δ are considered as control inputs

of the system; thus, the new equation is non-linear and time-variant.

$$\frac{d}{dt}\begin{bmatrix} i_d \\ i_q \\ V_{dc} \end{bmatrix} = \begin{bmatrix} \frac{-r}{L} & \omega & \frac{-m\cos\delta}{\sqrt{3}L} \\ -\omega & \frac{-r}{L} & \frac{-m\sin\delta}{\sqrt{3}L} \\ \frac{\sqrt{3}m\cos\delta}{2C} & \frac{\sqrt{3}m\sin\delta}{2C} & \frac{-1}{RC} \end{bmatrix} \times \begin{bmatrix} i_d \\ i_q \\ V_{dc} \end{bmatrix} + \begin{bmatrix} \frac{1}{L} \\ 0 \\ 0 \end{bmatrix} E_d \quad (12)$$

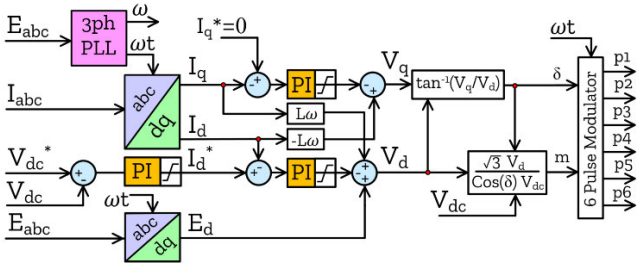

FIGURE 6. Classic controller based on three PI regulator applicable for SR.

There are three main objectives for controller design for SR: Tracking desired DC voltage (V_{dc}^*) while supplying the demanded active power and reducing the reactive power to zero. A classic control technique based on PI regulator satisfies each one of the objectives through three PI controller loops. The detailed structure of the PI-based controller is depicted in Fig. 6. First of all, instantaneous values of E_{abc} are delivered to the PLL block to extracting the online frequency (ω) and phase (ωt) values of the power network. All the measured three-phase currents (I_{abc}) are transformed into the rotational reference frame (I_d & I_q). This transformation is done for E_{abc} to E_d as well. Tracking the DC voltage is the main part of the control system, and the first PI produces the desired value of direct access current (I_d^*) from ΔV_{dc} error signal. Naturally, I_q^* is zero to have only active component. The remained part of the control scheme comes from (7), where the target is to produce two compensator phrases (ΔV_d *and* ΔV_q) to generate the correct values of V_d and V_q.

$$\begin{cases} V_d = L\omega i_q + E_d - \Delta V_d \\ V_q = -L\omega i_d - \Delta V_q \end{cases} \quad (13)$$

The pulse width modulator for driving the converter needs to receive m and $\omega t + \delta$, which after calculation of V_d and V_q can be generated from (11). Both of m and δ are bounded values ($0< m <1$ and $|\delta| < 90^\circ$), and it must be considered in control loops. Also, the output of the voltage control loop (I_d^*) is considered a bounded value as well, due to the nominal limitation of the converter's structure. Therefore by increasing the coefficients of PI controllers (K_P and K_I), to have a faster response, the system will be saturated. To illustrate this, a series of detailed simulations

TABLE 1. Simulation parameters.

Item	Value
E_{an} (v)	23
X (Ω) @50Hz	0.5
r (Ω)	0.1
R (Ω)	25
C (μf)	4700
V_{dc}^* (v) step change	100 → 120

have been performed in MATLAB-SIMULINK environment according to the simulation parameters listed in Table (1). To examine dynamic response of the controller, a step-change in desired DC voltage has been applied in the fourth second from 100V to 120V. The results are illustrated in Fig. 7. The unsaturated response of the controller is shown in Fig. 7(a).

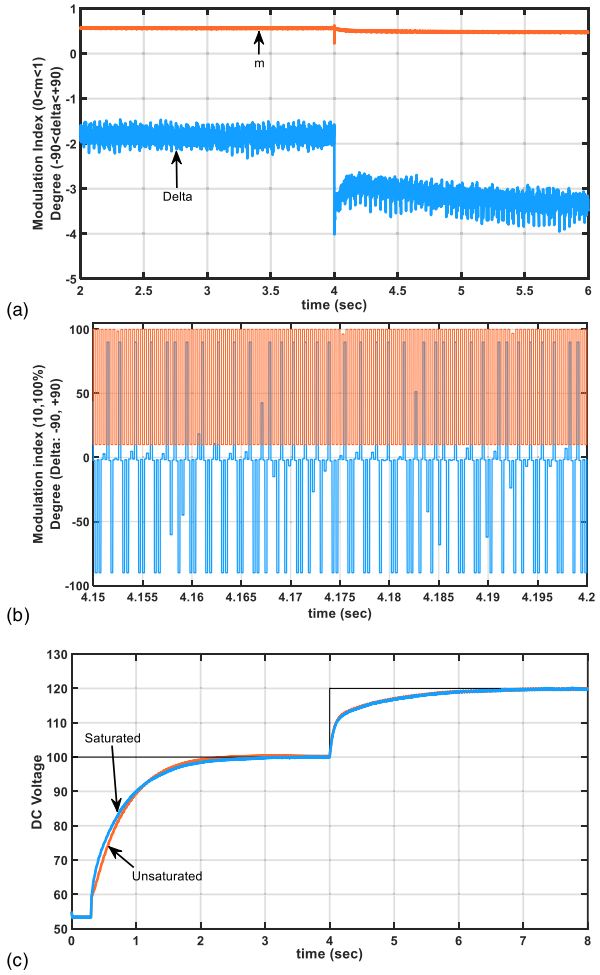

FIGURE 7. Simulation results of step-change in DC voltage: (a) Unsaturated m and δ, (b) Saturated m and δ, (c) V_{dc}.

After increasing the PI coefficients by 20%, both of controller outputs are saturated in Fig. 7(b). Oscillations of m and δ between upper and lower bands are clear while there is no significant difference between output DC voltages, Fig. 7(c). This result shows that the PI controller has no sense of saturation, and the further increase of the coefficients may lead

to instability. Moreover, compensation of parameter uncertainties and estimation of disturbances are other concerns in a proper controller. By considering the variation of DC load as an external disturbance in the non-linear state-space equation (12) and including unknown uncertainties, integral terminal sliding mode controller and disturbance-observer concepts are raised in the next section.

III. CONTROLLER DESIGN

Consider the generalized form of a relative-degree-one uncertain non-linear system as:

$$\dot{x} = f(x) + \Delta f(x) + (g(x) + \Delta g(x))\, u + d_0(t) \tag{14}$$

where x is the state of the system, f and g denote the non-linear functions. In addition, uncertainties are shown by Δf and Δg. The external disturbance and control input are respectively presented by d_0 and u. Considering all uncertain terms and the external disturbance as a single disturbance term $d(t)$, the equation of the system is:

$$\begin{aligned} \dot{x}(t) &= f(x) + g(x)\, u + d(t) \\ d(t) &= \Delta f(x) + \Delta g(x)\, u + d_0(t) \end{aligned} \tag{15}$$

To proceed with the design of integral terminal sliding mode control (ITSMC) for the three-phase power converter, lemma 1 is required [26].

Lemma 1: Let $V(t)$ as a continuous positive definite function. If $V(t)$ fulfils the following condition:

$$\dot{V}(t) + \vartheta V(t) + \xi V^{\chi} \leq 0, \quad \forall t > t_0 \tag{16}$$

Then as a result, $V(t)$ converges to the equilibrium point in a finite time t_s:

$$t_s \leq t_0 + \frac{1}{\vartheta(1+\chi)} \ln \frac{\vartheta V^{1-\chi}(t_0) + \xi}{\xi} \tag{17}$$

where $\vartheta > \xi > 0$ and $0 < \chi < 1$.

A. FAST DISTURBANCE OBSERVER

The fast disturbance-observer is applied to approximate the unknown external loads and uncertainties. The output of the disturbance observer is used in the control input formulation. To design a finite time disturbance observer, the following auxiliary variables are defined [27].

$$s_d = z - x \tag{18}$$

Also, the derivative of variable z is given by:

$$\dot{z} = -k s_d - \beta sign(s_d) - \varepsilon s_d^{\frac{p_0}{q_0}} - |f(x)|\, sign(s_d) + g(x)\, u \tag{19}$$

where k and ε are positive and $\beta > |d|$. Also p_0 and q_0 are odd positive integers and $p_0 < q_0$. The disturbance estimation $(\hat{d})$ is given by:

$$\hat{d} = -k s_d - \beta sign(s_d) - \varepsilon s_d^{\frac{p_0}{q_0}} - |f(x)|\, sign(s_d) - f(x) \tag{20}$$

According to Eqs. (15), (18), and (19) we have:

$$\begin{aligned} \dot{s_d} = \dot{z} - \dot{x} = -k s_d - \beta \text{sign}(s_d) - \varepsilon s_d^{\frac{p_0}{q_0}} \\ - |f(x)| \text{ sign}(s_d) - f(x) - d \end{aligned} \tag{21}$$

considering Eqs. (19) and (20), disturbance approximation error $(\tilde{d})$ can be achieved:

$$\begin{aligned} \tilde{d} &= \hat{d} - d \\ &= -k s_d - \beta \text{sign}(s_d) - \varepsilon s^{\frac{p_0}{q_0}} - |f(x)| \text{ sign}(s_d) - f(x) - d \\ &= -k s_d - \beta sign(s_d) - \varepsilon s_d^{\frac{p_0}{q_0}} - |f(x)|\, sign(s_d) \\ &\quad - f(x) - \dot{x} + f(x) + g(x)\, u \\ &= -k s_d - \beta sign(s_d) - \varepsilon s_d^{\frac{p_0}{q_0}} - |f(x)|\, sign(s_d) \\ &\quad + g(x)\, u - \dot{x} \\ &= \dot{z} - \dot{x} = \dot{s_d} \end{aligned} \tag{22}$$

Theorem 1: Considering the uncertain non-linear system (14), by applying fast disturbance observer (18)-(20), the disturbance approximation error (22) converges to zero in the finite time.

Proof: Let the Lyapunov function as:

$$V_1 = \frac{1}{2} s_d^2 \tag{23}$$

The derivative of the Lyapunov function (V_1) gives:

$$\begin{aligned} \dot{V}_1 &= s_d \dot{s}_d = s_d \left(-k s_d - \beta sign(s_d) - \varepsilon s_d^{\frac{p_0}{q_0}} \right. \\ &\quad \left. - |f(x)|\, sign(s_d) - f(x) - d \right) \\ &\leq -k s_d^2 - \beta s_d \text{sign}(s_d) - \varepsilon s_d^{\frac{p_0+q_0}{q_0}} - |f(x)|\, s_d sign(s_d) \\ &\quad - s_d f(x) - s_d d \\ &\leq -k s_d^2 - \beta |s_d| - \varepsilon s_d^{\frac{p_0+q_0}{q_0}} - |f(x)|\, |s_d| - s_d f(x) \\ &\quad + |s_d|\, |d| \leq -k s_d^2 - \varepsilon s_d^{\frac{p_0+q_0}{q_0}} \leq -2kV_1 \\ &\quad - 2^{(p_0+q_0)/2q_0} \varepsilon V_1^{(p_0+q_0)/2q_0} \end{aligned} \tag{24}$$

Thus, according to Lemma 1 and Eq. (24), the s_d converges to zero in the finite time. Then, as a result, $\dot{s_d} = 0$ and based on Eq. (22), the disturbance approximation error $\tilde{d}$ converges to zero in finite time.

Remark 1: Based on the Theorem 1 and Lemma 1, the convergence time of the disturbance approximation error is:

$$t_{sd} < t_0 + \frac{q_0}{k(p_0 + 3q_0)} \ln \left(\frac{k(s_d(t_0))^{(q_0 - p_0)/q_0}}{\varepsilon} + 1 \right) \tag{25}$$

where t_0 indicates the initial time.

B. INTEGRAL TERMINAL SLIDING MODE CONTROL

The tracking error of system (14) is defined as $e = x - x_d$. In this study, the integral terminal sliding surface is constructed as:

$$s_t(t) = s_d(t) + e(t) + \sigma \int_0^t e(t)^{\frac{p}{q}} dt \tag{26}$$

To improve the robus performance of conventional sliding mode, the integral sliding mode approach has been developed [28], [29]. Add an integral term to the sliding mode controller results in a highly accurate control against both parametric variations and chattering reduction [30], [31]. This way, the idea of integral sliding mode focuses on the system robustness in the entire state space rather than only in the sliding phase [32]. The order of the motion equation in integral sliding mode method is equal to the dimension of the state space. Therefore, the robustness performance can be guaranteed through the entire response of the system. Due to its capability, the integral sliding mode has gained significant attention, and it has also been proposed for unmatched and matched uncertain systems [33].

The control input of the disturbance-observer-based ITSMC is proposed as follows:

$$u = -\frac{1}{g(x)}\left(f(x) - \dot{x}_d + \hat{d} + \varsigma s_t + \mu s_t^{\frac{p_1}{q_1}} + \sigma e^{\frac{p}{q}}\right) \quad (27)$$

where ς, μ and σ are positive design parameters, p_1, q_1, p, and q are odd numbers.

Theorem 2: The suggested disturbance-observer-based ITSM guarantees the stability of the closed-loop system, the convergence of the tracking error in the presence of the external disturbances, and modeling uncertainties.

Proof: The Lyapunov functional $V_2(t)$ is formed as:

$$V_2 = \frac{1}{2}s_t^2 \quad (28)$$

Taking the derivative of the Lyapunov function yields:

$$\begin{aligned}\dot{V}_2 &= s_t\left(\dot{s}_d + \dot{e}(t) + \sigma e^{\frac{p}{q}}\right) = s_t\left(\dot{s}_d + \dot{x} - \dot{x}_d + \sigma e^{\frac{p}{q}}\right)\\ &= s_t\left(\dot{s}_d + f(x) + g(x)u + d - \dot{x}_d + \sigma e^{\frac{p}{q}}\right) \quad (29)\end{aligned}$$

using the control law (27), we have:

$$\begin{aligned}\dot{V}_2 &= s_t\left(\dot{s}_d - \dot{x}_d + f(x) - f(x) - \hat{d} - \delta s_t - \mu s_t^{\frac{p_1}{q_1}}\right.\\ &\quad \left. -\sigma e^{\frac{p}{q}} + d + \dot{x}_d + \sigma e^{\frac{p}{q}}\right)\\ &= s_t\left(\dot{s}_d + d - \hat{d} - \varsigma V_2 s_t - \mu s_t^{\frac{p_1}{q_1}}\right) \quad (30)\end{aligned}$$

Considering Eq. (22):

$$\begin{aligned}\dot{V}_2 &= s_t\left(-\varsigma s_t - \mu s_t^{\frac{p_1}{q_1}}\right)\\ &= -\varsigma s_t^2 - \mu s_t^{\frac{p_1+q_1}{q_1}} \le -2\varsigma V_2 - 2^{\frac{p_1+q_1}{2q_1}}\mu V_2^{\frac{p_1+q_1}{q_1}} \quad (31)\end{aligned}$$

Thus, it is concluded from Lemma 1 and Eq. (31), that $s_t(x) = s_d(x) + e(t) + \sigma\int_0^t e(t)^{\frac{p}{q}}dt$ converges to zero in a finite time (T_s). The value of T_s can be easily calculated based on Lemma 1. Hence, the system converges to the sliding surface in a finite time. Also, $s_d(x)$ converges to zero in finite time (as it was mentioned in the previous section). Therefore, after a finite time system is on the sliding surface, and results in $e(t) + \sigma\int_0^t e(t)^{\frac{p}{q}}dt = 0$. By defining the dynamic error equation as: $e_I(t) = \int_0^t e(t)^{\frac{p}{q}}dt$, on the sliding surface, we have $\dot{e}_I(t) = -(\sigma e_I)^{\frac{p}{q}}$. Solving the dynamic error equation leads to the calculation of the convergent time of $e_I(t)$ as follows:

$$T_f = \frac{|e_I(t_s)|^{1-\frac{p}{q}}}{\sigma^{\frac{p}{q}}(1-\frac{p}{q})} = \frac{|e(t_s)|^{1-\frac{p}{q}}}{\sigma^{\frac{p}{q}+1}(1-\frac{p}{q})} \quad (32)$$

Meanwhile, the spent time for the convergence of the tracking error $e(t)$ is T_f. To recapitulate briefly, from Lemma 1 and (32) it can be calculated that the tracking error e converges to the zero in the finite time.

Remark 2: In the proposed control scheme (ITSMC), there is not the sign function for the sliding surface in the control input. We have the sign function for the variable s_d, where s_d is the variable regarded to the disturbance observer. ITSMC stabilizes the system in the finite time; therefore, the sliding surface converges to zero in finite time. Thus, the function of sign(s_d) will be zero after a short time, and the chattering and vibration are reduced/eliminated during the stabilization of the system by employing the ITSMC. In fact, the ITSMC possesses two advantages: (a) Stabilizing the system in the finite time, and (b) Reducing/Eliminating the chattering from the signal control input. Therefore, the vibration in the system will be reduced.

C. ITSMC WITH INPUT SATURATION

Due to physical limitations, control input saturation may occur in many real systems. Thus, in the current study, the disturbance-observer-based ITSMC with unknown input saturation is developed. By applying the input saturation constraints, the control input u is as follow:

$$u = \Gamma(u_c) \quad (33)$$

where u_c is the control input command and will be designed in the following. The function $\Gamma(.)$ denotes an unknown saturation function. By defining $\tilde{u} = u - u_c$ and substituting into Eq. (15) we have:

$$\begin{aligned}\dot{x}(t) &= f(x) + g(x)(u_c + \tilde{u}) + d\\ &= f(x) + g(x)u_c + D \quad (34)\end{aligned}$$

where $D = g(x)\tilde{u} + d$ is all of the disturbances expose to the system in the presence of control input saturation. According to section 3.a, the fast disturbance observer is designed as:

$$\hat{D} = -ks_d - \beta sign(s_d) - \varepsilon s_d^{\frac{p_0}{q_0}} - |f(x)|\,sign(s_d) - f(x) \quad (35)$$

where s_d is defined in Eq. (18) and z will be obtained by:

$$\dot{z} = -ks_d - \beta sign(s_d) - \varepsilon s_d^{\frac{p_0}{q_0}} - |f(x)|\,sign(s_d) + g(x)u_c \quad (36)$$

where the parameter β should be designed as $\beta > |D|$. According to Theorem 1, the approximation error of the disturbance observer converges to zero in the finite time. Consequently, for the system (14), the disturbance observer-based

ITSMC (DOB-ITSM) in the presence of the control input saturation is designed as:

$$u_c = -\frac{1}{g(x)}\left(f(x) - \dot{x}_d + \hat{D} + \varsigma s_t + \mu s_t^{\frac{p_1}{q_1}} + \sigma e^{\frac{p}{q}}\right) \quad (37)$$

where $s_t(t)$ is expressed in Eq. (26).

Theorem 3: Consider the non-linear system (14) in the presence of external disturbance and control input saturation. Using the control input (37), the tracking error of the closed-loop system converges to zero in the finite time.

Proof: Let Lyapunov function as:

$$V_3 = \frac{1}{2}s_t^2 \quad (38)$$

The derivative of V_3 yields:

$$\begin{aligned}\dot{V}_3 &= s_t\left(\dot{s}_d + e\dot{(}t) + \sigma e^{\frac{p}{q}}\right) = s_t\left(\dot{s}_d + \dot{x} - \dot{x}_d + \sigma e^{\frac{p}{q}}\right)\\ &= s_t\left(\dot{s}_d + f(x) + g(x)u_c + D - \dot{x}_d + \sigma e^{\frac{p}{q}}\right) \quad (39)\end{aligned}$$

substituting the proposed control law (37), into Eq.(39) yields:

$$\begin{aligned}\dot{V}_3 = s_t\Big(&\dot{s}_d - \dot{x}_d + f(x) - f(x) - \hat{D} - \varsigma s_t - \mu s_t^{\frac{p_1}{q_1}} - \sigma e^{\frac{p}{q}}\\ &+ D + \dot{x}_d + \sigma e^{\frac{p}{q}}\Big) = s_t\left(\dot{s}_d + D - \hat{D} - \varsigma s_t - \mu s_t^{\frac{p_1}{q_1}}\right) \quad (40)\end{aligned}$$

According to Eq. (22), we know $D - \hat{D} = -\dot{s}_d$; therefore:

$$\begin{aligned}\dot{V}_3 &= s_t\left(-\varsigma s_t - \mu s_t^{\frac{p_1}{q_1}}\right) = -\varsigma s_t^2 - \mu s_t^{\frac{p_1+q_1}{q_1}}\\ &\le -2\varsigma V_3 - 2^{\frac{p_1+q_1}{2q_1}}\mu V_3^{\frac{p_1+q_1}{q_1}} \quad (41)\end{aligned}$$

Thus, based on Eq. (41) and Lemma 1, the tracking error e converges to the zero in a finite time. This demonstrates that using the proposed controller, the tracking error of the uncertain closed-loop system converges to the zero even in the presence of control input limitation.

To briefly recapitulate the design procedure of the controller parameters, all the parameters must be designed in such a way that they satisfy stability condition which is as: $\beta > |D|$, p, q, p_0 and q_0 are odd positive integers in which $p_0 < q_0$ and $p < q$. Moreover, parameters ς, μ, σ, k, and ε should be positive.

D. VOLTAGE REGULATION LOOP

The governing equation of the voltage regulation loop is as follow:

$$\frac{dV_{dc}}{dt} = \frac{\sqrt{3}m\cos(\delta)}{2C}i_d + \frac{\sqrt{3}m\sin(\delta)}{2C}i_q - \frac{1}{RC}V_{dc} \quad (42)$$

As it is mentioned in [34], the current dynamics are much faster than the voltage dynamics. Also, based on the singular perturbation theory, in the designing controller process for the voltage regulation loop, we can assume $i_d \cong i_d^*$ and $i_q \cong i_q^*$. This assumption yields [35].

$$\frac{dV_{dc}}{dt} = \frac{1}{V_{dc}}\left(P^* - P_{load}\right) \quad (43)$$

where $P^* = \frac{\sqrt{3}\,m\cos(\delta)}{2C}i_d^*V_{dc} + \frac{\sqrt{3}\,mSin(\delta)}{2C}i_q^*V_{dc}$. Moreover, $P_{load} = \frac{V_{dc}^2}{RC}$ denotes an unknown time-varying external disturbance. By defining the variable $w = V_{dc}^2/2$, and substituting in Eq. (43):

$$\frac{dw}{dt} = P^* - P_{load} \quad (44)$$

Comparing the generalized form of a relative-degree-one uncertain non-linear system Eq. (14) and Eq.(44), it is obvious that for the voltage regulation loop $f(x) = 0$ and $g(x) = 1$. Hence, P^* is the control input for the voltage regulation loop and will be designed in the following. According to section 3.a, the disturbance-observer for the voltage regulation loop is given by:

$$\begin{aligned}\hat{D}_w &= -ks_{dw} - \beta\,\mathrm{sign}(s_{dw}) - \varepsilon s_{dw}^{\frac{p_0}{q_0}}\\ \dot{z}_w &= -ks_{dw} - \beta\,\mathrm{sign}(s_{dw}) - \varepsilon s_{dw}^{\frac{p_0}{q_0}} + P^*\\ s_{dw} &= z_w - w \quad (45)\end{aligned}$$

We consider the regulation error as $e_w = w - w^*$ where $w^* = \frac{V_{dc}^{*2}}{2}$ and V_{dc}^* is the desired value of the voltage. Then, based on the proposed method, the integral terminal sliding surface for the voltage regulation loop is constructed as:

$$s_w = s_{dw}(t) + e_w(t) + \sigma\int_0^t e_w(t)^{\frac{p}{q}}dt \quad (46)$$

Based on the proposed control technique, P^* is as follow:

$$P^* = \Gamma\left(-\left(-\dot{w}^* + \hat{D}_w + \varsigma s_w + \mu s_w^{\frac{p_1}{q_1}} + \sigma e_w^{\frac{p}{q}}\right)\right) \quad (47)$$

Fig. 8 illustrates the block diagram of the disturbance-observer- based ITSMC for voltage regulation loop.

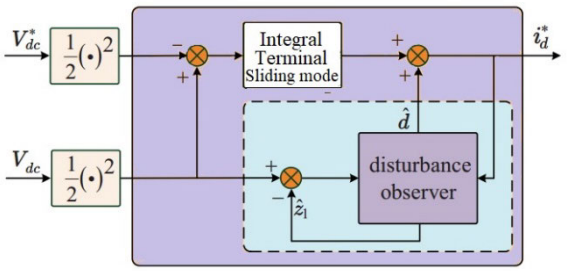

FIGURE 8. Illustration of voltage regulation loop with disturbance-observer- based ITSMC.

E. CURRENT TRACKING LOOP

From (12), the governing equation of the current tracking loop is as follows:

$$\begin{aligned}\frac{di_d}{dt} &= -\frac{r}{L}i_d + \omega i_q - \frac{u_d}{\sqrt{3}\,L}V_{dc} + \frac{E_d}{L}\\ \frac{di_q}{dt} &= -\omega i_d - \frac{r}{L}i_q - \frac{u_q}{\sqrt{3}\,L}V_{dc} \quad (48)\end{aligned}$$

where $u_d = m\cos(\delta)$ and $u_q = m\sin(\delta)$. The currents i_q, and i_d should track their references i_q^* and i_d^*, respectively.

The reference value i_q^*, is set to provide a desired instantaneous reactive power ($q^*= 0$). Also, the reference value i_d^* is calculated in order to dc-link capacitor voltage is regulated to the desired value (V_{dc}^*). Hence, the current references are given by:

$$i_d^* = \frac{P^*}{v_d} \quad i_q^* = 0 \tag{49}$$

The tracking errors are considered as:

$$\begin{aligned} e_d &= i_d - i_d^* \\ e_q &= i_q - i_q^* \end{aligned} \tag{50}$$

The current tracking loop controller based on the proposed method in the presence of the input saturation is given by:

$$\begin{aligned} u_d = \Gamma\Bigg(-\frac{\sqrt{3}L}{V_{dc}}\Bigg(-\frac{r}{L}i_d + \omega i_q - \frac{d}{dt}i_d^* + \varsigma_d s_{td} \\ + \mu_d s_{td}^{\frac{p_{d1}}{q_{d1}}} + \sigma_d e_d^{\frac{p_d}{q_d}}\Bigg)\Bigg) \end{aligned} \tag{51}$$

$$\begin{aligned} u_q = \Gamma\Bigg(-\frac{\sqrt{3}L}{V_{dc}}\Bigg(-\omega i_d - \frac{r}{L}i_q - \frac{d}{dt}i_q^* + \varsigma_q s_{tq} \\ + \mu_q s_{tq}^{\frac{p_{q1}}{q_{q1}}} + \sigma_q e_q^{p_q/q_q}\Bigg)\Bigg) \end{aligned} \tag{52}$$

where the sliding surfaces for the current tracking loop are:

$$\begin{aligned} s_{td} &= s_{dd}(t) + e_d(t) + \sigma_d \int_0^t e_d(t)^{\frac{p_d}{q_d}} dt \\ s_{tq} &= s_{dq}(t) + e_q(t) + \sigma_q \int_0^t e_q(t)^{\frac{p_q}{q_q}} dt \end{aligned} \tag{53}$$

It should be mentioned that the disturbance observer only used for the voltage regulation loop. Actually, the disturbance observer which used for the voltage regulation loop detects load disturbances. The parameters of the control scheme should be designed such that they satisfy the stability conditions, described in Sections 3.a, 3.b, and 3.c. The control scheme is shown in Fig. 9 for the current tracking loop with disturbance-observer-based ITSM.

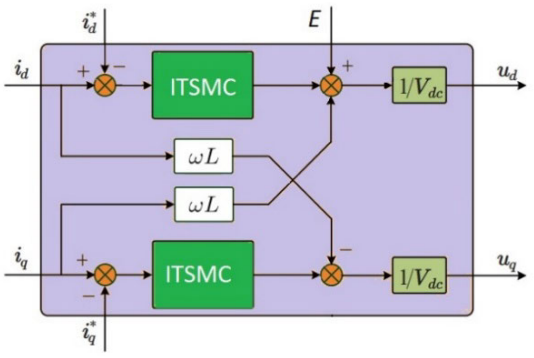

FIGURE 9. Illustration of current tracking loop with disturbance-observer-based ITSMC.

F. CHOOSING CONTROL PARAMETERS

According to the proposed control technique, there are three control loops which they contain several parameters.

According to Fig. 8, the outputs of the voltage regulation loops act as the control inputs for the current tracking loops. Hence, due to the importance of the current tracking loop, at first, the parameter of these control loops should be assigned.

Remark 3: To reach a high performance of the control scheme, the value of currents (i_d and i_q) should be convergent to their desired value in a short time. Consequently, according to Eq. (41) and Lemma1 we should consider relatively large value for parameters δ_d, δ_q, μ_d, and μ_q. It is noteworthy that a very large value can be selected for these parameters, but sometimes large parameters may enhance the chattering in the system response and control signals. Hence, choosing parameters is a trade-off. When the current tracking loops act appropriately, the parameters of the voltage regulation loop could be easily designed to obtain the best response of the system. All these parameters are tuned after running several detailed simulations. In the designing of the proposed controller, all signals, including disturbances and states of the system, are considered to be bunded, which is a common assumption in designing a controller for practical systems. However, may the bound of compound disturbance be unknown. Hence, a relatively high value for β should be selected. The control parameters for voltage regulation loop, including disturbance observer parameters and two current control loops, i_d and i_q, are listed in Tab. 2. All the presented results in the next section have been extracted with these parameters.

TABLE 2. The control parameters.

voltage regulation loop				current tracking loop (i_d)		current tracking loop (i_q)	
Par	Value	Par	Value	Par	Value	Par	Value
k	29	p	1	σ_d	3	σ_q	1
β	5	q	1	p_d	1	p_q	1
ε	10	ς	27	q_d	1	q_q	1
p_0	1	μ	300	ς_d	400	ς_q	450
q_0	3	p_1	1	μ_d	10	μ_q	450
σ	300	q_1	11	p_{d1}	1	p_{q1}	1
				q_{d1}	11	q_{q1}	13

IV. SIMULATION AND EXPERIMENTAL RESULTS

The general structure of the proposed control technique is developed in Fig. 10, based on the conventional model, which has been discussed in Fig. 6.

The voltage regulation loop is replaced with the proposed disturbance observer, surrounded by dash line, and two other PI loops are replaced by ITSMC. To demonstrate the performance ability of the proposed controller in real condition, an AC power source impregnated with low order harmonics is assumed both in simulation and real experiment. The real waveform of the three-phase source along with frequency

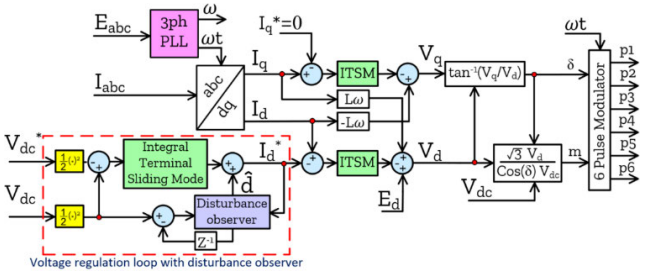

FIGURE 10. General control diagram with DO and ITSMC.

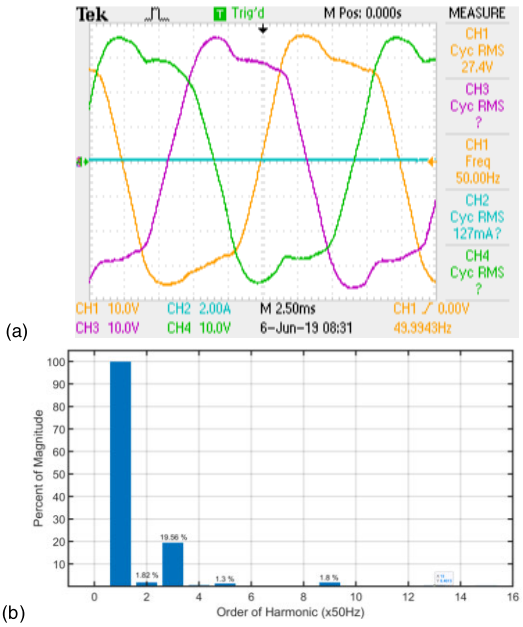

FIGURE 11. (a) Three-phase waveform of power source, (b) Frequency spectrum analysis of three-phase waveform.

spectrum analysis, is shown in Fig. 11. To generate the appropriate pulses for the power converter, Discontinuous Pulse Width Modulator (DPWM 60°) is applied. The duty cycle pattern of three different m is shown in Fig. 12(a). Despite the harmonic style of each individual pattern, the relative duty cycles are pure sinusoidal shape, Fig. 12(b).

A. SIMULATION RESULTS

To have a better understanding of the proposed control technique and before real implementation, a series of detailed simulation has been done in MATLAB-SIMULINK. Simulations are done for both conventional PI controller and ITSMC. Two types of dynamic responses are examined, step-change in V_{dc}^* and step change in the load resistance as an external disturbance. The results of the step-change of V_{dc}^* are compared in Fig. 13. The better performance of ITSM is obvious, while no saturation happens.

The results of the step-change of DC load are compared in Fig. 14. Three levels of load resistor (50,100 and 25Ω) are changed in step format while $V_{dc}^* = 100$V. In the proposed control scheme, the load variation is considered as external

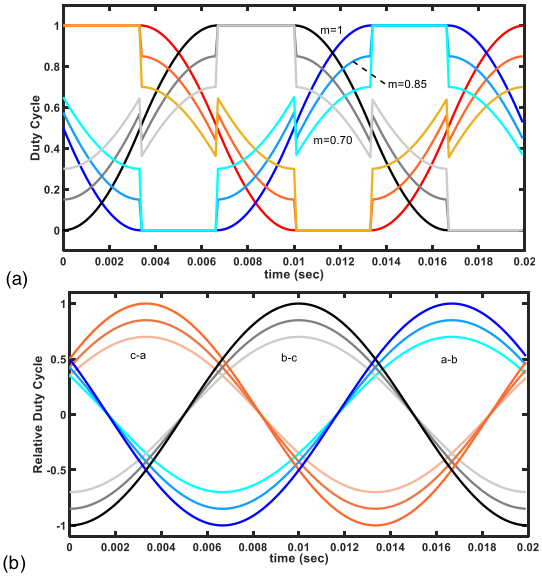

FIGURE 12. (a) three-phase discontinuous duty cycle pattern for specified m_{abc}, (b) relative duty cycle pattern.

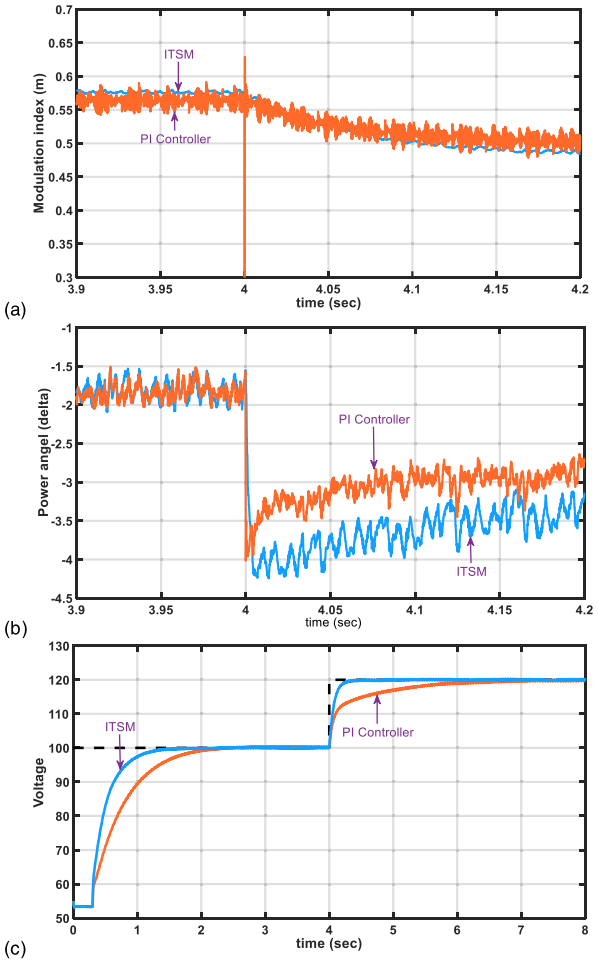

FIGURE 13. Simulation results: Performance comparison between ITSM and PI controller due to step changing in V_{dc}^*. (a) Modulation index, (b) Power angle (δ in degree), (c) V_{dc}.

disturbance, and it has been tracked by an observer. The output of the voltage control loop is considered as a reference

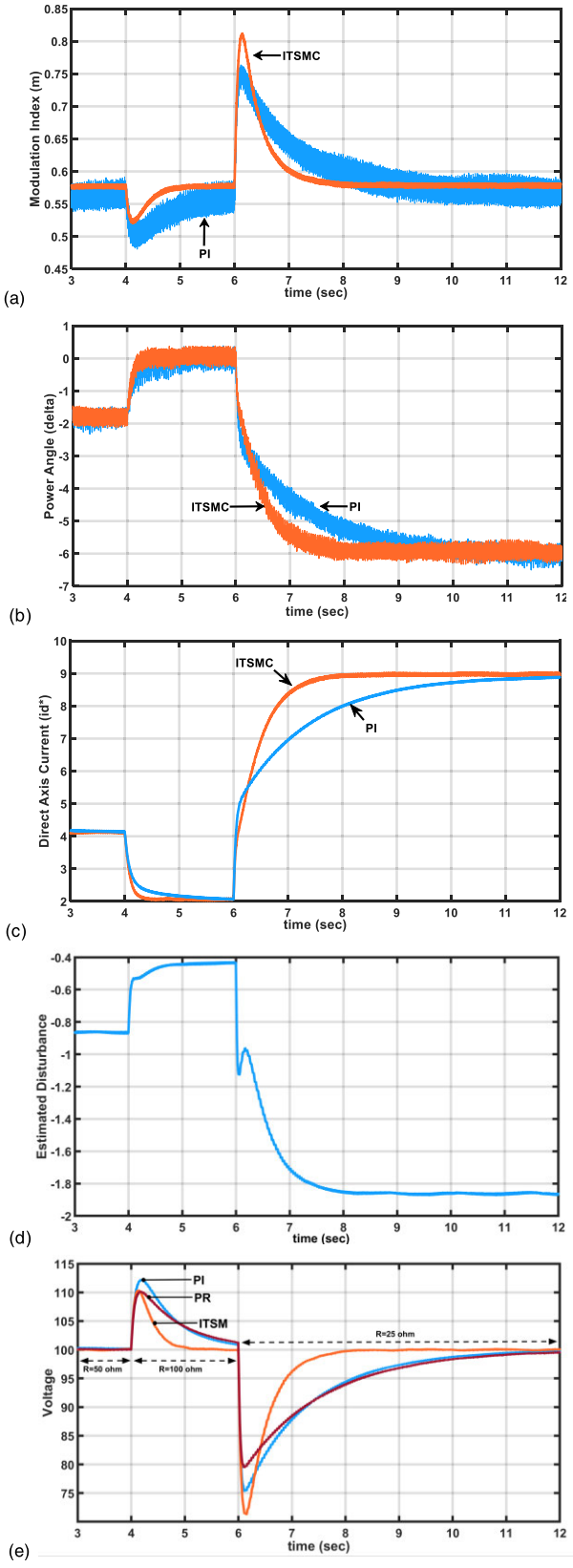

FIGURE 14. Simulation results: Performance comparison between ITSM and PI controller due to step changing in DC load. (a) Modulation index, (b) Power angle (δ in degree), (c) output of voltage control loop (I_d*), (d) estimated disturbance, (e)V_{dc}(including the PR controller performance).

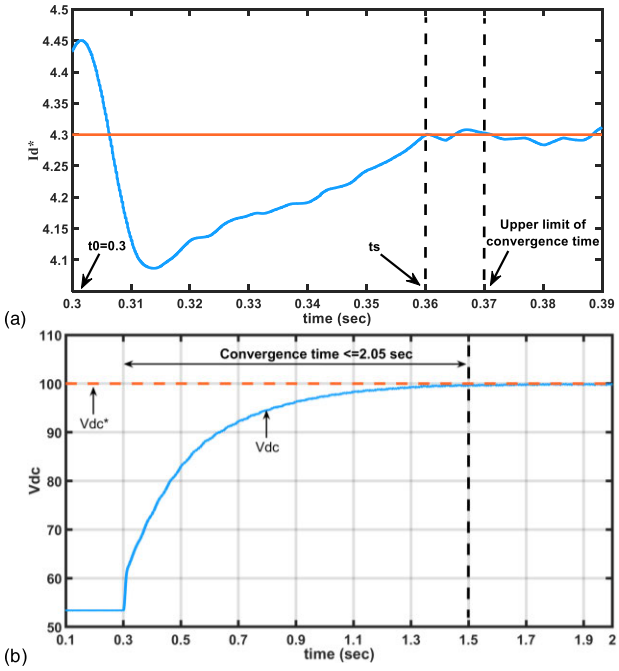

FIGURE 15. Finite-time convergence in (a) voltage control loop (DO) and (b) current control loop.

value for the direct axis current control loop (I_d^*). The generated values for I_d^* due to both PI and DOB-ITSM are depicted in Fig. 14(c). The normalized estimated disturbance by the observer is shown in Fig.14(d). To have a better validation, a separate simulation in $\alpha\beta$ frame, based on [1], is done with PR controller and the output waveform is compared with two other performances, PI and DOB-ITSMC, in Fig.14(e).

The outstanding performance of the proposed controller is clear in tracking V_{dc} to the desired value.

According to the proof of the finite-time convergence, the convergence time for each one of three controllers consists of two parts, convergence to the sliding surface and convergence the sliding surface to the equilibrium point which they are depended to an initial state of errors and sliding surface before every dynamic response or disturbances. The amount of these initial values must be obtained from the simulated model. According to the parameters of TAB. 2 and considering the start time as t_0= 0.3, the maximum values for the convergence time of the current and voltage control loops (DO) are calculated in Appendix I. The performance of DO in tracking the load current steps is shown in Fig. 15(a). The maximum calculated convergence time is $T_{T_{V_{dc}}} = 0.071sec$. The observer converged to the new load current (4.3A) in 0.06 sec, which is smaller than 0.07 sec. The performance of the ITSM in the current loop in tracking the variation of V_{dc} is shown in Fig. 15(b). The current controller converged to the new V_{DC}^* (100V) in 1.2 sec, which is smaller than 2.05 sec.

B. EXPERIMENTAL RESULTS

To examine the validity of the proposed control technique, an experimental setup has been prepared according to Fig. 16.

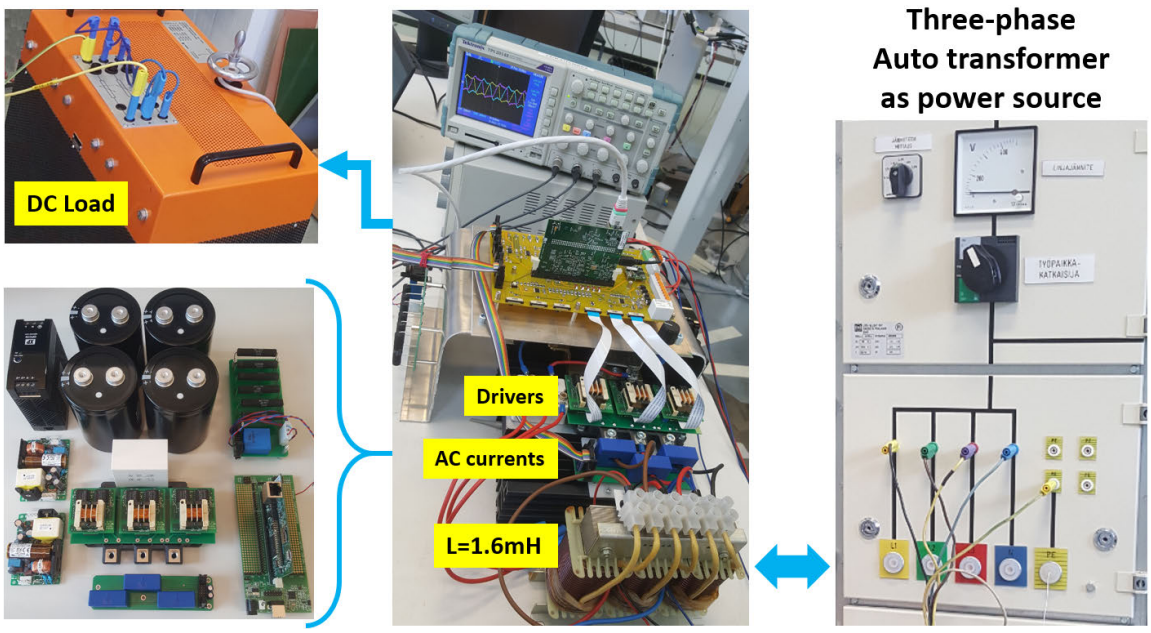

FIGURE 16. Experimental setup of synchronous rectifier.

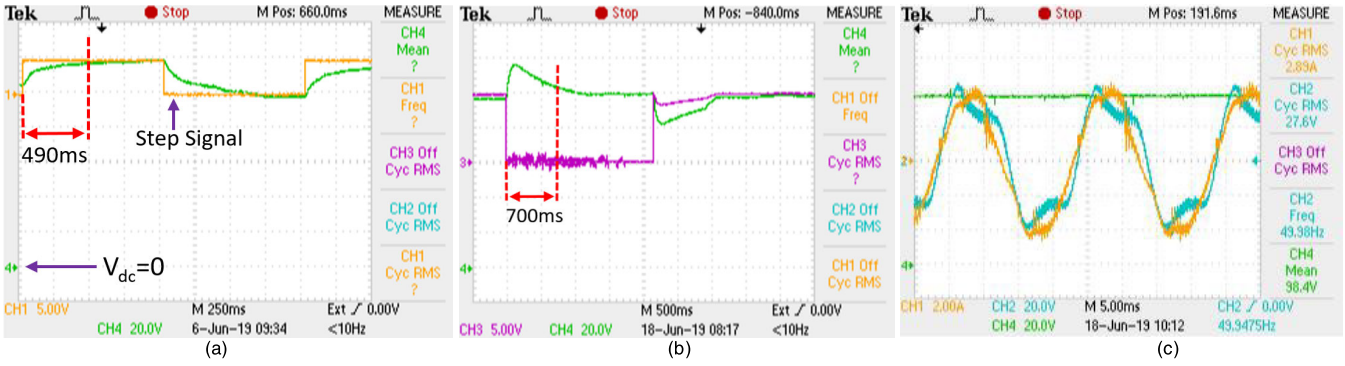

FIGURE 17. Experimental results: Performance of ITSM controller, (a) step change in V_{dc}*, (b) step change in DC load, (c) current is in phase with corresponding voltage.

All the parameters are the same as in the simulation environment. An autotransformer is used as a power source, and two-core processor (F28M35) is utilized for real-time implementation. DSP core is dedicated to reading the analogue data (voltage and currents), executing the control algorithms, and controlling the PWMs while the other core (ARM type) acts as a data transceiver between MATLAB and DSP core. Similar to the simulation section, two types of dynamic response evaluations are performed here as well, a step-change in the desired DC voltage and a step-change in the load. A periodic symmetrical 0.25Hz pulse with a lower level of 100V and upper level of 120V is used as a step input of the control loop. The recorded data due to step-change in V_{dc}^*, for both PI and ITSMC, can be compared in Figs. 17(a) and 18(a). The performance of ITSMC over PI controller is evident. The response of ITSM to tracking the V_{dc}^* approximately two times faster than PI. To analyze the dynamic behavior of SR due to load variations, another 50Ω resistor is connected to a fixed 50Ω load through an on/off switch. The performance of ITSMC is compared with the PI controller in Figs. 17(b) and 18(b). Zero reactive power is one of the control constrains, which is fulfilled in both control techniques. Comparison of voltage and current of AC power source for one of the three-phase indicates that they are in phase with each other for ITSMC as well as PI controller, Figs.17(c) and 18(c). Because of the distorted waveform of power source, a very small displacement between voltage and current is visible. But in general, perfect in-phase matching between voltage and current is evident.

C. SPECIFICATIONS OF THE PROPOSED CONTROLLER

In the presented control technique, near to 26 parameters must be tuned for the observer and three control loops, while the conventional PI control scheme only depends on six parameters. At the first look, it seems such a complicated technique and two substantial questions will be raised.

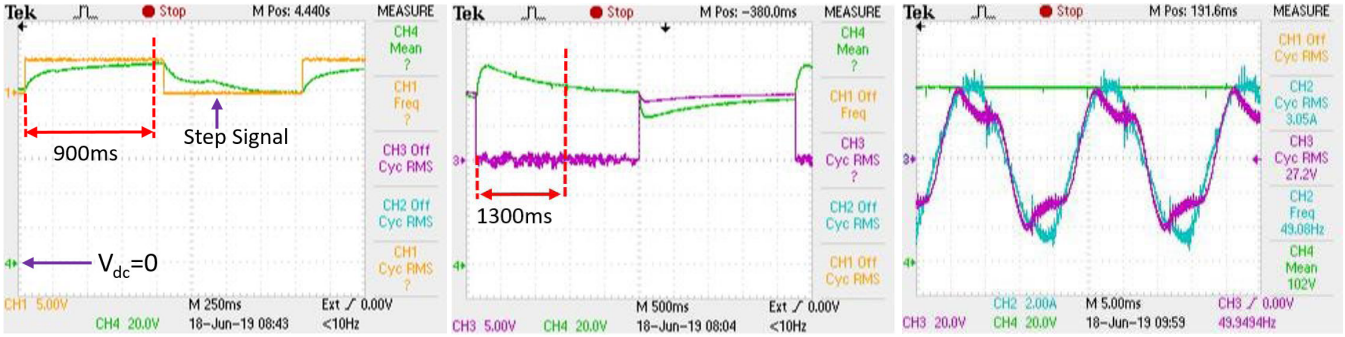

FIGURE 18. Experimental results: Performance of PI controller, (a) step change in V_{dc}*, (b) step change in DC load. (c) current is in phase with corresponding voltage.

How to set parameters, and what is the benefit? Despite a large number of control parameters, it is not difficult to find the appropriate values for them. According to the described algorithm in section 3.F and doing some of simulations, the proper values for parameters are achievable. Actually, In comparison to a conventional control scheme, increasing the number of parameters is a cost to have the following benefits:

1- Stable and robust performance against uncertainties and load disturbances.
2- Finite-time convergence of the system tracking error.
3- Quick response for tracking the reference values.
4- Preserved stability in the presence of control input saturation.

V. CONCLUSION

A new control structure of three-phase synchronous rectifier was developed based on the integral terminal sliding mode controller. The proposed control technique was implemented on a non-linear and time-varying model of a three-phase grid-connected converter in the conventional synchronous reference frame. DC-load variation was considered as an external disturbance. Therefore, a disturbance observer was utilized to estimate the active power and consequently to produce the amount of direct axis reference value for the current control loop. The proposed controller has Four outstanding features, robust performance against uncertainties and load disturbances, finite-time convergence of the closed-loop system tracking error, quick response in tracking reference values and mathematically proven and experimentally confirmed stability in the presence of control input saturation. By performing a series of detailed and precise simulations along with a real-time implementation on a laboratory setup of a three-phase synchronous rectifier, the validity of the proposed control scheme was fully investigated and confirmed. As a future suggestion, the developed disturbance observer can be promoted via a fuzzy logic system. The appropriate performance possibility of the proposed controller suggests the extension of the application of this method for other power converters. Also, future studies could also be devoted to combining neural networks and fuzzy systems with the proposed controller. This way, the controller will possess the advantages of neural networks and fuzzy systems.

APPENDIX

Here, as an example, the convergence of the system from the starting point of the controller (T = 0.3 sec) is calculated. The maximum convergence time for voltage and current control loops can be obtained as follows:

A. V_{DC}

The convergence time of the voltage loop can be obtained as follows:

$$T_{sV_{dc}} \leq 0.3 + \frac{1}{2\varsigma\left(1+\frac{p_1+q_1}{q_1}\right)} \times \ln\frac{2\varsigma s_w^{2\left(1-\frac{p_1+q_1}{q_1}\right)}(T_0) + 2^{\frac{p_1+q_1}{2q_1}}\mu}{2^{\frac{p_1+q_1}{2q_1}}\mu} = (0.3+0.001)\text{sec}$$

where $s_w(T_0) = 1.002$ comes from the simulation.

$$T_{fV_{dc}} = \frac{\left|e_w\left(T_{sV_{dc}}\right)\right|^{1-\frac{p_1}{q_1}}}{\sigma^{\frac{p_1}{q_1}+1}\left(1-\frac{p_1}{q_1}\right)} = 0.07\text{sec}$$

where $e_w\left(T_{sV_{dc}}\right) = -53$ comes from the simulation.

$$T_{TV_{dc}} \leq T_{sV_{dc}} + T_{fV_{dc}} = (0.301+0.07) = 0.371\text{sec}$$

B. i_d

$$T_{s_{id}} \leq 0.371 + \frac{1}{2\varsigma_d\left(1+\frac{p_{d1}+q_{d1}}{q_{d1}}\right)} \times \ln\frac{2\varsigma_d s_{td}^{2\left(1-\frac{p_{d1}+q_{d1}}{q_{d1}}\right)}(0.371) + 2^{\frac{p_{d1}+q_{d1}}{2q_{d1}}}\mu_d}{2^{\frac{p_{d1}+q_{d1}}{2q_{d1}}}\mu_d} = (0.371+0.0021) = 0.3731sec$$

where $s_{td}\,(0.371) = 27$ comes from the simulated model.

$$T_{f_{id}} = \frac{\left|e_d\left(T_{s_{id}}\right)\right|^{1-\frac{p_{d1}}{q_{d1}}}}{\sigma_d^{\frac{p_{d1}}{q_{d1}}+1}\left(1-\frac{p_{d1}}{q_{d1}}\right)} = 1.7sec$$

where $e_d\,(T_{sid}) = -6$ comes from the simulated model.

$$T_{T_{id}} \leq T_{s_{id}} + T_{f_{id}} = 0.3731 + 1.7 = 2.0731\text{sec}$$

C. i_q

$$\begin{aligned} T_{s_{iq}} &\leq 0.371 \\ &+ \frac{1}{2\varsigma_q\left(1+\frac{p_{q1}+q_{q1}}{q_{q1}}\right)} \\ &\times \ln\frac{2\varsigma_q s_{tq}^{\,1-\frac{p_{q1}+q_{q1}}{q_{q1}}}(0.371) + 2^{\frac{p_{q1}+q_{q1}}{2q_{q1}}}\mu_q}{2^{\frac{p_{q1}+q_{q1}}{2q_{q1}}}\mu_q} \\ &= (0.371 + 0.0034) = 0.3744sec \end{aligned}$$

where $s_{tq}\,(0.371) = 50$ comes from the simulated model.

$$T_{f_{iq}} = \frac{\left|e_q\left(T_{s_{iq}}\right)\right|^{1-\frac{p_{q1}}{q_{q1}}}}{\sigma_q^{\frac{p_{q1}}{q_{q1}}+1}\left(1-\frac{p_{q1}}{q_{q1}}\right)} = 2.05sec$$

where $e_q\left(T_{siq}\right) = 2$ comes from the simulated model.

$$T_{T_{iq}} \leq T_{s_{iq}} + T_{f_{iq}} = 0.3744 + 2.05 = 2.4244sec$$

The validity of the extracted convergence times can be checked by comparing them with the voltage and current waveforms in Fig.15.

REFERENCES

[1] F. Blaabjerg, R. Teodorescu, M. Liserre, and A. V. Timbus, "Overview of control and grid synchronization for distributed power generation systems," *IEEE Trans. Ind. Electron.*, vol. 53, no. 5, pp. 1398–1409, Oct. 2006.

[2] M. Barzegar-Kalashani, B. Tousi, M. A. Mahmud, and M. Farhadi-Kangarlu, "Non-linear integral higher-order sliding mode controller design for islanded operations of T-type three-phase inverter-interfaced distributed energy resources," *IET Gener., Transmiss. Distrib.*, vol. 14, no. 1, pp. 53–61, Jan. 2020.

[3] J. G. Hwang, P. W. Lehn, and M. Winkelnkemper, "A generalized class of stationary frame-current controllers for grid-connected AC–DC converters," *IEEE Trans. Power Del.*, vol. 24, no. 4, pp. 2742–2751, Oct. 2010.

[4] X. Zheng, Y. Li, Z. Liu, and C. Wang, "Steady-state control strategy of VSC-HVDC transmission system based on full-order terminal sliding mode control method," *J. Eng.*, vol. 2019, no. 16, pp. 987–990, Mar. 2019.

[5] C. Ren, X. Han, L. Wang, Y. Yang, W. Qin, and P. Wang, "High-performance three-phase PWM converter with a reduced DC-link capacitor under unbalanced AC voltage conditions," *IEEE Trans. Ind. Electron.*, vol. 65, no. 2, pp. 1041–1050, Feb. 2018.

[6] Z. Song, Y. Tian, Z. Yan, and Z. Chen, "Direct power control for three-phase two-level voltage-source rectifiers based on extended-state observation," *IEEE Trans. Ind. Electron.*, vol. 63, no. 7, pp. 4593–4603, Jul. 2016.

[7] J. Rocabert, A. Luna, F. Blaabjerg, and P. Rodríguez, "Control of power converters in AC microgrids," *IEEE Trans. Power Electron.*, vol. 27, no. 11, pp. 4734–4749, Nov. 2012.

[8] J. Liu, Y. Gao, W. Luo, and L. Wu, "Takagi–Sugeno fuzzy-model-based control of three-phase AC/DC voltage source converters using adaptive sliding mode technique," *IET Control Theory Appl.*, vol. 11, no. 8, pp. 1255–1263, May 2017.

[9] X. Zhang, Z. Fu, Y. Xiao, G. Wang, and D. Xu, "Control of parallel three-phase PWM converters under generalized unbalanced operating conditions," *IEEE Trans. Power Electron.*, vol. 32, no. 4, pp. 3206–3215, Apr. 2017.

[10] Z. Song, Y. Tian, W. Chen, Z. Zou, and Z. Chen, "Predictive duty cycle control of three-phase active-front-end rectifiers," *IEEE Trans. Power Electron.*, vol. 31, no. 1, pp. 698–710, Jan. 2016.

[11] Z. Zhou, P. Igic, P. J. Unsworth, and P. M. Holland, "Design and analysis of a feedforward control scheme for a three-phase voltage source pulse width modulation rectifier using sensorless load current signal," *IET Power Electron.*, vol. 2, no. 4, pp. 421–430, Jul. 2009.

[12] F.-J. Chang, E.-C. Chang, T.-J. Liang, and J.-F. Chen, "Digital-signal-processor-based DC/AC inverter with integral-compensation terminal sliding-mode control," *IET Power Electron.*, vol. 4, no. 1, pp. 159–167, 2011.

[13] M. B. Delghavi and A. Yazdani, "Sliding-mode control of AC voltages and currents of dispatchable distributed energy resources in master-slave-organized inverter-based microgrids," *IEEE Trans. Smart Grid*, vol. 10, no. 1, pp. 980–991, Jan. 2019.

[14] S. B. Santra, K. Kumar, P. Biswal, and C. K. Panigrahi, "Lyapunov based fast terminal sliding mode Q-V control of grid connected hybrid solar PV and wind system," *IEEE Access*, vol. 6, pp. 39139–39153, 2018.

[15] J. Liu, Y. Yin, W. Luo, S. Vazquez, L. G. Franquelo, and L. Wu, "Sliding mode control of a three-phase AC/DC voltage source converter under unknown load conditions: Industry applications," *IEEE Trans. Syst., Man, Cybern. Syst.*, vol. 48, no. 10, pp. 1771–1780, Oct. 2018.

[16] Y. Yin, J. Liu, J. A. Sanchez, L. Wu, S. Vazquez, J. I. Leon, and L. G. Franquelo, "Observer-based adaptive sliding mode control of NPC converters: An RBF neural network approach," *IEEE Trans. Power Electron.*, vol. 34, no. 4, pp. 3831–3841, Apr. 2019.

[17] W.-H. Chen, J. Yang, L. Guo, and S. Li, "Disturbance-observer-based control and related methods—An overview," *IEEE Trans. Ind. Electron.*, vol. 63, no. 2, pp. 1083–1095, Feb. 2016.

[18] S.-L. Shi, J.-X. Li, and Y.-M. Fang, "Extended-state-observer-based chattering free sliding mode control for nonlinear systems with mismatched disturbance," *IEEE Access*, vol. 6, pp. 22952–22957, 2018.

[19] R. Cui, L. Chen, C. Yang, and M. Chen, "Extended state observer-based integral sliding mode control for an underwater robot with unknown disturbances and uncertain nonlinearities," *IEEE Trans. Ind. Electron.*, vol. 64, no. 8, pp. 6785–6795, Aug. 2017.

[20] C. Hua, G. Liu, L. Zhang, and X. Guan, "Cooperative stabilization for linear switched systems with asynchronous switching," *IEEE Trans. Syst., Man, Cybern. Syst.*, vol. 49, no. 6, pp. 1081–1087, Jun. 2019.

[21] C.-C. Hua, K. Wang, J.-N. Chen, and X. You, "Tracking differentiator and extended state observer-based nonsingular fast terminal sliding mode attitude control for a quadrotor," *Nonlinear Dyn.*, vol. 94, no. 1, pp. 343–354, Oct. 2018.

[22] C. Hua, J. Chen, and X. Guan, "Fractional-order sliding mode control of uncertain QUAVs with time-varying state constraints," *Nonlinear Dyn.*, vol. 95, no. 2, pp. 1347–1360, Jan. 2019.

[23] M. Chen, Q.-X. Wu, and R.-X. Cui, "Terminal sliding mode tracking control for a class of SISO uncertain nonlinear systems," *ISA Trans.*, vol. 52, no. 2, pp. 198–206, Mar. 2013.

[24] S.-K. Kim, D.-K. Choi, K.-B. Lee, and Y. I. Lee, "Offset-free model predictive control for the power control of three-phase AC/DC converters," *IEEE Trans. Ind. Electron.*, vol. 62, no. 11, pp. 7114–7126, Nov. 2015.

[25] X. Zheng, Y. Feng, F. Han, and X. Yu, "Integral-type terminal sliding-mode control for grid-side converter in wind energy conversion systems," *IEEE Trans. Ind. Electron.*, vol. 66, no. 5, pp. 3702–3711, May 2019.

[26] M. Zhihong and X. H. Yu, "Terminal sliding mode control of MIMO linear systems," *IEEE Trans. Circuits Syst. I, Fundam. Theory Appl.*, vol. 44, no. 11, pp. 1065–1070, Nov. 1997.

[27] M. Chen, Q.-X. Wu, and R.-X. Cui, "Terminal sliding mode tracking control for a class of SISO uncertain nonlinear systems," *ISA Trans.*, vol. 52, no. 2, pp. 198–206, Mar. 2013.

[28] V. Utkin and J. Shi, "Integral sliding mode in systems operating under uncertainty conditions," in *Proc. 35th IEEE Conf. Decis. Control*, vol. 4, Dec. 1996, pp. 4591–4596.

[29] M. Rubagotti, D. M. Raimondo, A. Ferrara, and L. Magni, "Robust model predictive control with integral sliding mode in continuous-time sampled-data nonlinear systems," *IEEE Trans. Autom. Control*, vol. 56, no. 3, pp. 556–570, Mar. 2011.

[30] S. Li, H. Wang, Y. Tian, A. Aitouch, and J. Klein, "Direct power control of DFIG wind turbine systems based on an intelligent proportional-integral sliding mode control," *ISA Trans.*, vol. 64, pp. 431–439, Sep. 2016.
[31] A. Chihi, H. Ben Azza, M. Jemli, and A. Sellami, "Nonlinear integral sliding mode control design of photovoltaic pumping system: Real time implementation," *ISA Trans.*, vol. 70, pp. 475–485, Sep. 2017.
[32] R. Kumar, P. A. Chalanga, and B. Bandyopadhyay, "Smooth integral sliding mode controller for the position control of stewart platform," *ISA Trans.*, vol. 58, pp. 543–551, Sep. 2015.
[33] M. Furat and I. Eker, "Second-order integral sliding-mode control with experimental application," *ISA Trans.*, vol. 53, no. 5, pp. 1661–1669, Sep. 2014.
[34] F. Umbría, J. Aracil, F. Gordillo, F. Salas, and J. A. Sánchez, "Three-time-scale singular perturbation stability analysis of three-phase power converters," *Asian J. Control*, vol. 16, no. 5, pp. 1361–1372, Sep. 2014.
[35] J. Liu, S. Vazquez, L. Wu, A. Marquez, H. Gao, and L. G. Franquelo, "Extended state observer-based sliding-mode control for three-phase power converters," *IEEE Trans. Ind. Electron.*, vol. 64, no. 1, pp. 22–31, Jan. 2017.

BAHMAN ESKANDARI (Member, IEEE) received the B.Sc., M.Sc., and Ph.D. degrees in electrical engineering from the K. N. Toosi University of Technology (KNTU), Tehran, Iran, in 2003, 2006, and 2013, respectively. After his Ph.D., he joined Malayer University, Hamedan, Iran, as an Assistant Professor. He had a long term collaboration with the Advanced Power Electronics Laboratory (KNTU) in the field of flexible AC compensation in the power system as a Research Assistant, in 2014. He is currently a Postdoctoral Researcher with the Department of Electrical Engineering and Automation (EEA), Aalto University, Espoo, Finland. His research interests include design, implementing, control and modulation techniques for power electronic converters, and their application in a wide range of applications.

AMIN YOUSEFPOUR received the M.S. degree in mechanical engineering from the University of Tehran, Iran. Since 2015, he has been a Research Assistant with the Advanced Instrumentation Laboratory, University of Tehran. Also, up to now, he has done various projects in international collaboration with prestigious universities and research institutes. His research interests include control systems, robotics, reinforcement learning, and non-linear dynamics.

MOOSA AYATI received the B.Sc. degree in electrical engineering from the Isfahan University of Technology, Isfahan, Iran, in 2004, and the M.Sc. and Ph.D. degrees (Hons.) in electrical engineering from the K. N. Toosi University of Technology, Tehran, Iran, in 2006 and 2011, respectively. He spent two years as a Postdoctoral Fellow at the School of Electrical Engineering, College of Engineering, University of Tehran, Tehran, working on fault detection systems. He is currently the Head of the Advanced Instrumentation Laboratory (AIL) and an Associate Professor with the Control Division, School of Mechanical Engineering, College of Engineering, University of Tehran. His areas of interest include adaptive control and system identification, fault detection systems, instrumentation and industrial automation, mechatronics, and hybrid systems. He is a member of the Iranian Society of Instrumentation and Control, the Iranian Society of Mechanical Engineers, and the National Society of Mechatronics.

JORMA KYYRA (Member, IEEE) received the M.Sc., Lic.Sc., and D.Sc. degrees from the Helsinki University of Technology (TKK), in 1987, 1991, and 1995, respectively. Since 1985, he has been with the university in various positions. Since 1996, he has also been an Associate Professor of power electronics, and since 1998, he has also been a Professor of power electronics. From 2008 to 2009, he had been the Dean of the Faculty of Electronics, Communications and Automation, TKK. From 2009 to 2011, he was the Vice President of Aalto University, Espoo, Finland. He is currently the Head of the Department of Electrical Engineering and Automation, Aalto University. His research interest is power electronics at large. The power electronics group at Aalto University has expertise, e.g., in power electronics for ac drives, dc-dc converters, modeling of converters, filtering of EMI, power factor correction, and distributed power systems.

EDRIS POURESMAEIL (Senior Member, IEEE) received the Ph.D. degree in electrical engineering from the Technical University of Catalonia (UPC-Barcelona Tech), Barcelona, Spain, in 2012. After his Ph.D., he joined the University of Waterloo, Waterloo, ON, Canada, as a Postdoctoral Research Fellow and then joined the University of Southern Denmark (SDU), Odense, Denmark, as an Associate Professor. He is currently an Associate Professor with the Department of Electrical Engineering and Automation (EEA), Aalto University, Espoo, Finland. His main research interests include application of power electronics in power and energy sectors.